Synthesis and Ligand Exchange of Thiol-Capped Silicon Nanocrystals

ARTICLE *in* LANGMUIR · MAY 2015

Impact Factor: 4.46 · DOI: 10.1021/acs.langmuir.5b01246 · Source: PubMed

4 AUTHORS, INCLUDING:

Yixuan Yu

University of Texas at Austin

18 PUBLICATIONS **114** CITATIONS

SEE PROFILE

Clare E Rowland

Northwestern University

19 PUBLICATIONS **234** CITATIONS

SEE PROFILE

Langmuir

Article

pubs.acs.org/Langmuir

Synthesis and Ligand Exchange of Thiol-Capped Silicon Nanocrystals

Yixuan Yu,[†] Clare E. Rowland,[‡,§] Richard D. Schaller,[‡,§] and Brian A. Korgel*,[†]

[†]McKetta Department of Chemical Engineering, Texas Materials Institute, and Center for Nano- and Molecular Science and Technology, The University of Texas at Austin, Austin, Texas 78712-1062, United States

[‡]Department of Chemistry, Northwestern University, 2145 Sheridan Road, Evanston, Illinois 60208, United States

[§]Center for Nanoscale Materials, Argonne National Laboratory, 9700 South Cass Avenue, Argonne, Illinois 60439, United States

Supporting Information

ABSTRACT: Hydride-terminated silicon (Si) nanocrystals were capped with dodecanethiol by a thermally promoted thiolation reaction. Under an inert atmosphere, the thiol-capped nanocrystals exhibit photoluminescence (PL) properties similar to those of alkene-capped Si nanocrystals, including size-tunable emission wavelength, relatively high quantum yields (>10%), and long radiative lifetimes (26−280 μs). X-ray photoelectron spectroscopy (XPS) and Fourier transform infrared (FTIR) spectroscopy confirmed that the ligands attach to the nanocrystal surface via covalent Si−S bonds. The thiol-capping layer, however, readily undergoes hydrolysis and severe degradation in the presence of moisture. Dodecanethiol could be exchanged with dodecene by hydrosilylation for enhanced stability.

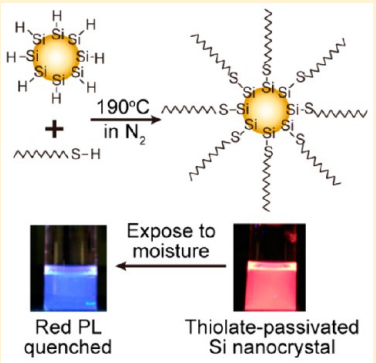

INTRODUCTION

Silicon (Si) is an extraordinarily useful semiconductor, employed in a wide variety of commercial applications, including transistors, optical detectors, and solar cells, yet is a very poor light emitter.[1] By creating quantum dots, Si can be made to emit light efficiently with color that can be tuned with size from near-infrared to visible wavelengths.[2−5] These optical properties make Si quantum dots an earth-abundant alternative to toxic cadmium (Cd)- and lead (Pb)-containing nanocrystal light emitters.[6,7] Si is also biodegradable[7] and offers other unique electronic and thermoelectric properties[8] that are potentially useful for a range of applications, such as imaging contrast agents,[6,7,9,10] sensors,[7] light-emitting diodes,[11,12] photovoltaic devices,[13−15] thin-film transistors,[16,17] and optical displays,[18] to name a few.[2,19]

Colloidal quantum dots are stabilized using molecular (typically organic) capping ligands to prevent oxidation and corrosion, provide dispersibility in solvents, and prevent aggregation.[20,21] Thus far, the most common and effective approach to capping Si nanocrystals involves the addition of alkenes by hydrosilylation.[3,10,22−30] This provides good stabilization of the luminescence, even in the presence of air, but the hydrocarbon ligands are covalently and irreversibly bonded to the Si surface, which makes synthesis by arrested precipitation from Si reactants impossible in the presence of alkenes and prevents further manipulations, as in the deposition of an inorganic shell or an exchange of capping ligands. In this context, amines have shown some promise as a labile ligand for Si; for example, dodecylamine has been applied as a capping ligand for Si nanorod synthesis aided with tin and gold seed particles.[30−33] However, amines have been shown to significantly influence the optical properties of Si nanocrystals.[34−36]

Here, we show that alkanethiols can be used as capping ligands for Si nanocrystals and allow for ligand exchange with alkenes. Alkanethiols have been used extensively as capping ligands on many other types of nanocrystals but not Si.[37−41] We find that thiol-capped Si nanocrystals exhibit size, crystallinity, and PL properties similar to those of the alkene-passivated Si nanocrystals but are very susceptible to hydrolysis and degradation in the presence of moisture. Dodecanethiol could also be exchanged with alkenes by a subsequent thermally promoted hydrosilylation reaction.

MATERIALS AND METHODS

Materials. FOx-16 was purchased from Dow Corning. 1-Dodecanethiol [$CH_3(CH_2)_{11}SH$ > 98%], anhydrous toluene (C_7H_8), anhydrous ethanol (C_2H_5OH), and anhydrous methanol (CH_3OH) were purchased from Sigma-Aldrich. Ethanol, chloroform, and hydrochloric acid (HCl, 37.5%) were obtained from Fisher Scientific. Hydrofluoric acid (HF, 48%) was obtained from EMD Chemical. Deionized (DI) water was obtained using a Barnstead Nanopure Filtration System (17 MΩ resistance).

Si Nanocrystal Synthesis and Ligand Exchange. Hydride-terminated Si nanocrystals were synthesized using published procedures.[3,42] In a typical synthesis, 30 mL of FOx-16 is evaporated under vacuum in a Schlenk line to form a white residue of hydrogen silsesquioxane (HSQ). This is heated under forming gas (93% N_2 gas and 7% H_2 gas) flow at 1100−1250 °C for 1 h. Nanocrystals with

Received: April 7, 2015
Revised: May 27, 2015
Published: May 29, 2015

DOI: 10.1021/acs.langmuir.5b01246
Langmuir 2015, 31, 6886−6893

diameters of about 2.5, 5.0, and 8.0 nm are obtained by heating at 1100, 1200, and 1250 °C, respectively. The reaction product is ground with agate mortar and pestle for 30 min and then shaken in a wrist-action shaker for 9 h with 3 mm borosilicate glass beads to create a fine, brown powder. This powder is etched with 48% HF and 37.5% HCl (10:1, v/v) in the dark for 4–6 h. Hydride-terminated Si nanocrystals are isolated from the HF etching solution by centrifugation at 8000 rpm for 5 min, followed by rinses with ethanol (twice) and chloroform. The nanocrystals are dispersed in 1-dodecanethiol (~1 mL/1 mg of nanocrystals). Then, in a three-neck flask on a Schlenk line, the dispersion is put through three freeze–pump–thaw cycles and heated to 190 °C with N_2 gas flow for 12 h. The initially turbid dispersion gradually becomes optically clear. The reaction is cooled, and the flask is sealed and moved to a nitrogen-filled glovebox. The nanocrystal dispersion is centrifuged at 8000 rpm for 5 min, and the supernatant is collected. The nanocrystals are then precipitated with anhydrous ethanol and centrifugation. The precipitate is collected and redispersed with anhydrous toluene. This washing procedure is carried out 2 more times. The yield of thiol-passivated Si nanocrystals depends upon the nanocrystal size, with yields of nearly 100, 80, and 20% for nanocrystals with diameters of 2.5, 5.0, and 8.0 nm, respectively. For ligand exchange, dodecanethiol-capped silicon nanocrystals were dispersed in 1-dodecene in a three-neck flask. The solution was degassed by freeze–pump–thaw cycles and heated to 190 °C in nitrogen gas for 12 h.

Material Characterization. Photoluminescence (PL) spectra were acquired on a Fluorolog-3 spectrophotometer (Horiba Jobin Yvon) with a charge-coupled device (CCD) detector for visible detection and an InGaAs photomultiplier tube for near-infrared (NIR) detection. PL spectra were obtained from Si nanocrystals dispersed in anhydrous toluene in 10 mm path-length quartz cuvettes. Time-resolved PL derived from time-correlated single-photon counting (TCSPC) were collected by exciting the sample in a 1 mm cuvette using a 35 ps pulse width, 405 nm diode laser operated between 1 kHz and 40 MHz. PL was focused into a fiber optic running to a 300 mm grating spectrograph using a quartz lens. Time-resolved dynamics were obtained using a single-photon sensitive avalanche photodiode and time-to-amplitude converter. The TCSPC data were fit to a biexponential decay.

$$I = A_1 e^{-t/\Gamma_1} + A_2 e^{-t/\Gamma_2} \quad (1)$$

Transmission electron microscopy (TEM) images were acquired digitally using a FEI Tecnai Biotwin transmission electron microscope operated at 80 kV accelerating voltage or a JEOL 2010F transmission electron microscope operated at 200 kV. Nanocrystal samples were prepared by drop casting toluene dispersions onto a 200 mesh carbon-coated copper grid (Electron Microscopy Science). Some TEM images were obtained on graphene supports using previously described methods.[43]

X-ray diffraction (XRD) data were obtained on a Rigaku R-Axis Spider diffractometer with a two-dimensional (2D) image plate detector, a graphite monochromator, and Cu Kα radiation (λ = 0.154 18 nm). XRD samples were prepared by drying the nanocrystals on a glass slide and transferring them to a nylon loop with a needle. Mineral oil was applied to secure the sample as needed. Diffraction data were collected for 60 min while rotating the sample stage at 10° min^{-1}. The 2D diffraction data were radially integrated with 2DP Spider software (version 1.0, Rigaku Americas Corp.)

Attenuated total reflectance Fourier transform infrared (ATR–FTIR) spectra were obtained on a Thermo Mattson Infinity Gold FTIR spectrometer with a Spectra-Tech Thermal ARK attenuated total reflectance module. The sample and detector chambers were purged with N_2 for 30 min to eliminate the CO_2 background signal. Nanocrystals dispersed in anhydrous toluene with a concentration of ~5 mg/mL were drop-cast onto the crystal plate of the ARK module and dried in N_2 gas flow. Both measurements and background scans were made by acquiring 512 scans at a resolution of 4 cm^{-1}. The average transmittance is reported with the background subtracted.

X-ray photoelectron spectroscopy (XPS) was measured with Kratos Axis Ultra XPS, using monochromatic Al Kα X-rays ($h\nu$ = 1486.5 eV) at 150 W (10 mA and 15 kV), hybrid optics (employing a magnetic and electrostatic lens simultaneously), and a multichannel plate coupled to a hemispherical photoelectron kinetic analyzer. The instrument work function is calibrated to give a binding energy (BE) of 368.3 eV for the Ag $3d_{5/2}$ line for metallic silver. Spectra were charge-corrected to the main line of the carbon 1s spectrum of Super P carbon (graphite-like carbon) set to 284.5 eV. High-resolution XPS spectra were collected with a pass energy of 20 eV, at a 0.1 eV step. The base pressure in the analysis chamber was initially ~2×10^{-9} Torr but increased to ~4×10^{-8} Torr because of outgassing of the samples. Casa XPS analysis software (version 2.3.16 PR 1.6) was used for peak deconvolution, by applying a Shirley background and line shapes with a Gaussian (70%) and Lorentzian (30%) combination.[22] Samples were removed from a N_2-filled glovebox (~5 ppm of molecular oxygen) and immediately transferred to the ultrahigh-vacuum XPS chamber using an interface/capsule setup. This setup was designed and built at the Surface Analysis Laboratory of the Texas Materials Institute at The University of Texas at Austin to directly couple to the XPS chamber, allowing samples to only expose to an environment free of O_2 and moisture.

RESULTS AND DISCUSSION

Size, Crystallinity, and Optical Properties. The HSQ decomposition route used here to produce Si nanocrystals yields relatively uniform hydride-capped quantum dots with a diamond cubic Si crystal structure and controlled size.[3,29] The hydride-terminated surfaces provide an effective model system to study Si-capping ligand chemistry, in this case, the thermally promoted thiolation illustrated in Figure 1a. Because the size of the nanocrystals can affect Si surface reactivity,[22,44] three different average diameters were studied: 2.5, 5.0, and 8.0 nm. As the photographs in Figure 1b show, dispersions of hydride-terminated Si nanocrystals in dodecanethiol are very turbid and then become optically clear as the alkanethiol capping ligand layer forms on the nanocrystals. Figure 2 shows TEM images of the nanocrystals after thiol capping, which are well-dispersed and not aggregated (see the Supporting Information for TEM images of the nanocrystals prior to thiolation). The dodecanethiol-capped nanocrystals are brightly luminescent when kept in an inert environment, with size-dependent PL emission peak maxima. Figure 1c shows the PL emission spectra: the 2.5 nm nanocrystals emit at 720 nm (1.72 eV) and the 8.0 nm nanocrystals emit at 1010 nm (1.22 eV). These values are shifted to higher energy from the bulk band gap of Si of 1.1 eV as a result of quantum confinement. The PL lifetimes determined from TCSPC measurements (see Figure 1d) were also size-dependent. We obtained fitted lifetimes of 26.4, 81.8, and 282.6 μs for diameters of 2.5, 5.0, and 8.0 nm, respectively, which are similar to those of alkene-capped Si nanocrystals.[5,26]

The dodecanethiol-capped nanocrystals retain the diamond cubic crystal structure of the starting material, confirmed by XRD (Figure 3) and TEM (Figure 4). Each diffraction pattern in Figure 3 indexes to the diamond cubic crystal structure of Si. The observed crystalline lattice spacings in the TEM images in Figure 4 are also consistent with diamond cubic Si. Furthermore, the XRD peak widths in Figure 3 are consistent with the average particle diameters determined from the TEM images.

Capping Ligand Characterization and Stability. ATR–FTIR spectra and XPS were used to verify the bonding of dodecanethiol to the Si nanocrystals. Figure 5 shows a comparison of ATR–FTIR spectra for 1-dodecanethiol and dodecanethiol-capped Si nanocrystals. The 1-dodecanethiol

DOI: 10.1021/acs.langmuir.5b01246
Langmuir 2015, 31, 6886–6893

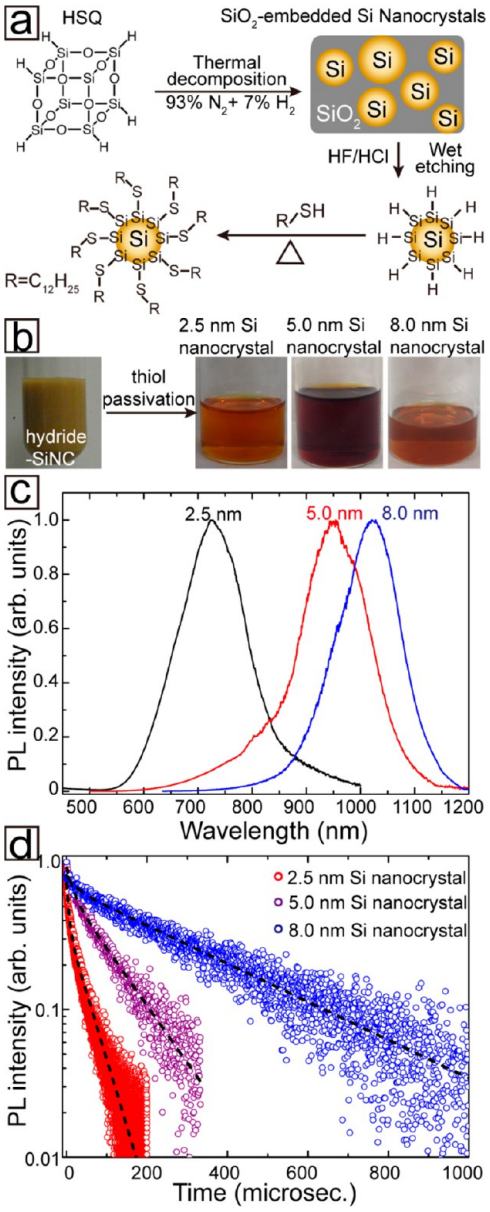

Figure 1. (a) Schematic description of the synthesis of dodecanethiol-capped Si nanocrystals. (b) Photographs of Si nanocrystal dispersions. The hydride-terminated Si nanocrystals form a turbid dispersion when initially added to 1-dodecanethiol and then form optically clear dispersions after thiolation has occurred. The dodecanethiol-capped Si nanocrystals have been isolated and redispersed in anhydrous toluene. (c) PL emission spectra of 2.5, 5.0, and 8.0 nm diameter dodecanethiol-capped Si nanocrystals photoexcited at 350, 400, and 420 nm, respectively. The PL intensities of the three samples are normalized in the plot. The PL quantum yield of the 2.5 nm nanocrystals was 12%. (d) TCSPC data of 2.5, 5.0, and 8.0 nm diameter dodecanethiol-capped Si nanocrystals dispersed in anhydrous toluene, which can be fitted with biexponential decay using eq 1, showing an average PL lifetime of 26.4, 81.8, and 282.6 μs for 2.5, 5.0, and 8.0 nm diameter dodecanethiol-capped Si nanocrystals, respectively.

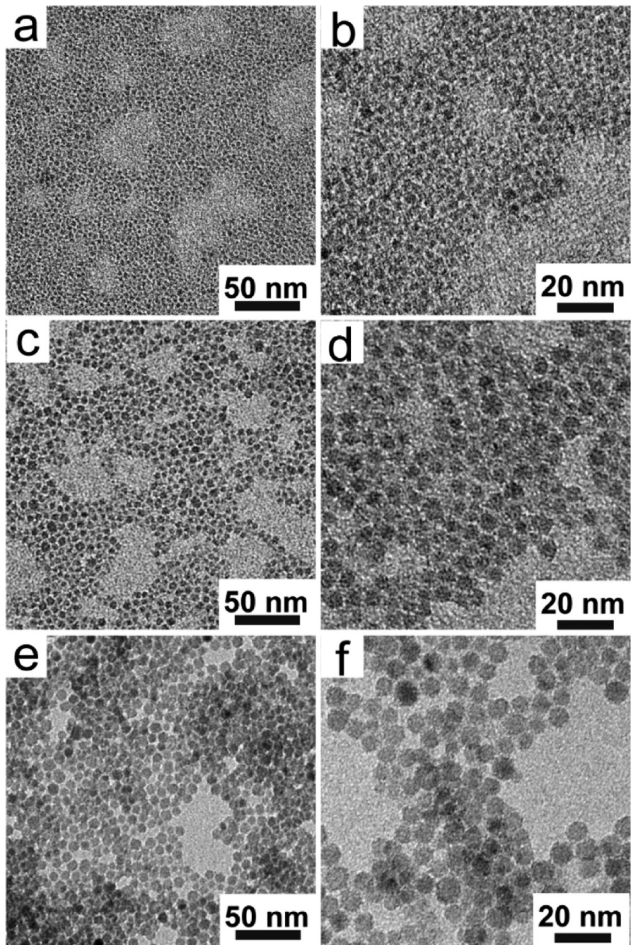

Figure 2. TEM images of dodecanethiol-capped Si nanocrystals with average diameters of (a and b) 2.5 nm, (c and d) 5.0 nm, and (e and f) 8.0 nm. TEM images of the hydride-terminated Si nanocrystals prior to thiolation are contained in the Supporting Information.

spectrum exhibits CH_3 stretching vibrations (asymmetric stretch at 2955 cm^{-1} and symmetric stretch at 2946–2879 cm^{-1}), CH_2 stretching vibrations (symmetric stretch at 2946–2879 cm^{-1} and symmetric stretch at 2850 cm^{-1}), C–H deformation vibrations between 1450 and 1250 cm^{-1}, C–S stretching vibration at 715 cm^{-1}, and a weak but detectable (see Figure 5b) S–H stretching vibration at 2575 cm^{-1}.[45] The dodecanethiol-capped Si nanocrystals exhibit C–H (both CH_3 and CH_2) and C–S vibrations similar to the 1-dodecanethiol spectra, with additional Si–H stretching vibrations between 2290 and 2240 cm^{-1}, Si–O stretching vibration at ~1100 cm^{-1}, and Si–H deformation vibration at 875 cm^{-1}.[45,46] The observation of Si–H in the spectra indicates that not all Si surface atoms can be passivated by the capping ligands as a result of steric hindrance in the ligand layer, which is also typical of Si nanocrystals after alkene passivation.[10,22] The absence of the S–H stretch in the nanocrystal spectra is consistent with attachment of dodecanethiol to the Si nanocrystal surface by S–H bond cleavage.[47]

XPS data also indicate that Si–S bonding occurs between the dodecanethiol-capping ligands and the Si surface through the formation of a Si–S bond. Figure 6 shows the XPS signal from the sulfur (S) 2p spectral region for the dodecanethiol-capped Si nanocrystals. The S $2p_{1/2}$ and S $2p_{3/2}$ doublet is present yet shifted from the free thiol value of 165 eV[48,49] for the S $2p_{1/2}$ peak to 163.8 eV for the 2.5 nm nanocrystals and 163.3 eV for the 5.0 nm nanocrystals. This size-dependent peak shift is also seen in thiolate-protected gold nanocrystals and has been attributed to the negative-charge-bearing sulfur atoms attached to the nanocrystal surface.[50,51]

DOI: 10.1021/acs.langmuir.5b01246
Langmuir 2015, 31, 6886–6893

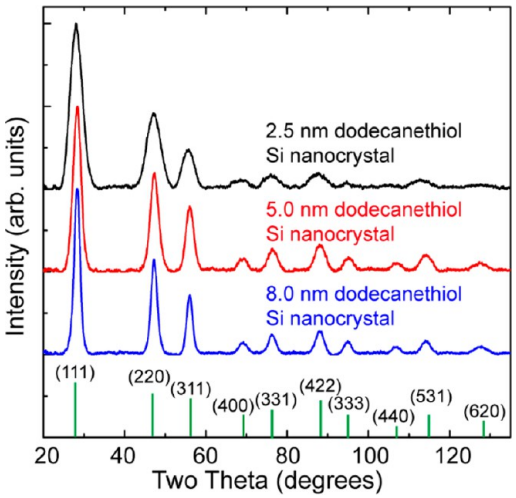

Figure 3. XRD data for dodecanethiol-capped Si nanocrystals. The average diameter of each sample is indicated, and a reference pattern is provided for diamond cubic Si (PDF 027-1402; a = b = c = 5.430 88 Å). All diffraction peaks are accounted for by indexing the pattern to diamond cubic Si. The average nanocrystal diameters determined from the XRD peaks by Debye−Scherrer analysis are 2.3, 4.6, and 7.5 nm, which are close to those determined by TEM (2.5, 5.0, and 8.0 nm). A description of the Scherrer equation calculations is provided in the Supporting Information.

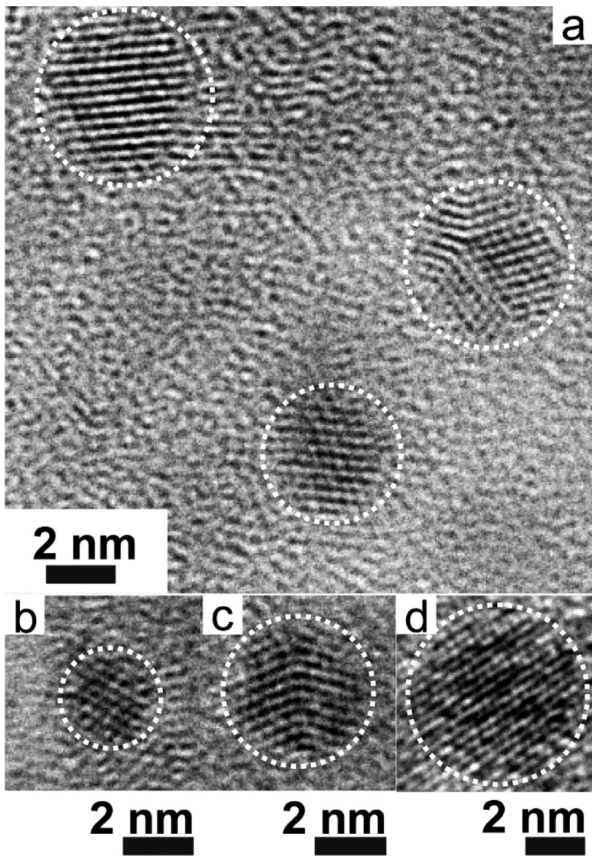

Figure 4. TEM images of dodecanethiol-capped Si nanocrystals from the samples with average diameters of (a) 5.0 nm, (b) 2.5 nm, (c) 5.0 nm, and (d) 8.0 nm.

Figure 7 shows the Si 2p XPS signal from the nanocrystals. The doublet expected from zero-valent Si at (Si^0 $2p_{1/2}$) 99.3 eV

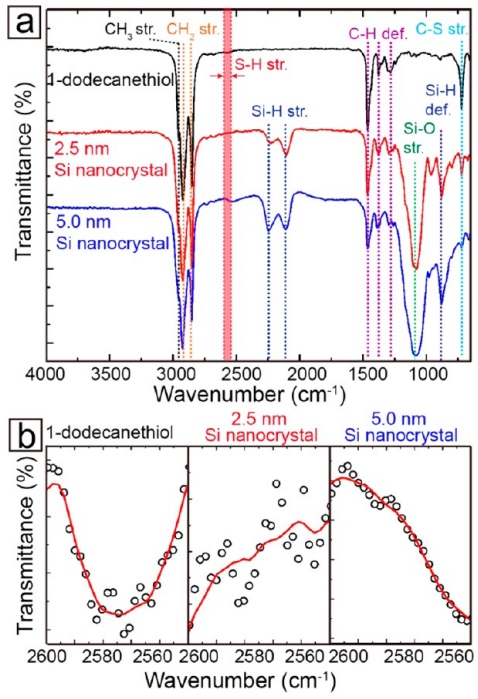

Figure 5. (a) ATR−FTIR spectra of 1-dodecanethiol compared to dodecanethiol-capped Si nanocrystals with average diameters of 2.5 and 5.0 nm. (b) ATR−FTIR spectral region between 2600 and 2550 cm^{-1} related to the S−H stretch.

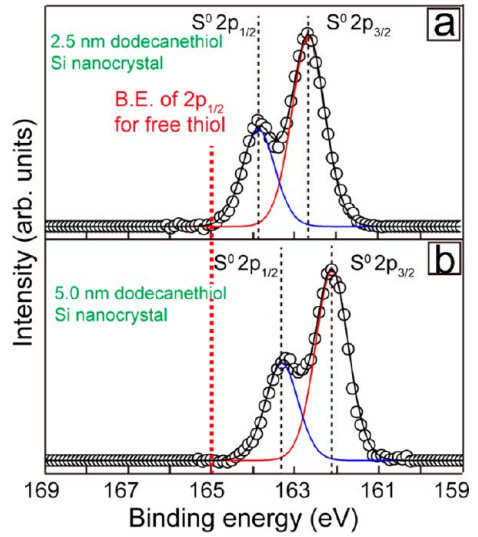

Figure 6. XPS S 2p spectra for 2.5 and 5.0 nm diameter dodecanethiol-capped Si nanocrystals. The S $2p_{1/2}$ and S $2p_{3/2}$ doublet is fitted using a 1:2 peak area ratio with the same full width at half maximum (fwhm) and 1.2 eV splitting.[49]

and (Si^0 $2p_{3/2}$) 99.8 eV is present, which further confirms that the thiolated nanocrystals are composed of zero-valent Si and have not been significantly oxidized or degraded during the thiolation procedure. We assign the significant peak at 101.9 eV to the Si−S bond between the capping ligands and the Si surface, following reports of the Si 2p binding energy of Si(100) with S adatoms.[52] As with alkene-treated Si nanocrystals, there is also some evidence of residual surface oxidation with small yet measurable contributions from various Si^{1+} (100.4 eV), Si^{2+} (101.5 eV), Si^{3+} (102.6 eV), and Si^{4+} (103.7 eV) species.[22]

DOI: 10.1021/acs.langmuir.5b01246
Langmuir 2015, 31, 6886−6893

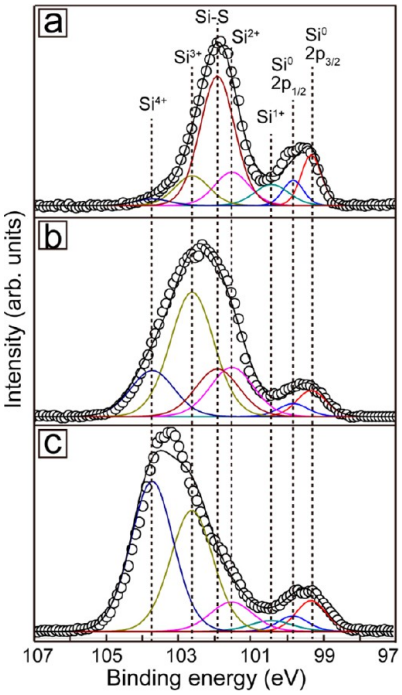

Figure 7. XPS Si 2p spectra for dodecanethiol-capped Si nanocrystals with 2.5 nm diameter (a) immediately after preparation, (b) after exposure to air for 4 days, and (c) after being dried in air for 5 h, showing various amounts of surface oxidation.

Panels b and c of Figure 7 show XPS data acquired after exposing the nanocrystals to air. The Si−S feature in the Si 2p region drops in intensity and completely disappears after drying in air. The signal in the S 2p region is also lost (see the Supporting Information), and Si^{3+} and Si^{4+} signals increase significantly as a result of surface oxidation in the absence of capping ligand protection. The instability of the thiolate-capping ligand layer in the presence of air is similar to that of SiS_x compounds.[53,54]

Exposing the dodecanethiol-capped Si nanocrystals to air also decreased the luminescence of the material. Figure 8 shows PL spectra of 2.5 nm diameter dodecanethiol-capped Si nanocrystals after exposure to air for 5 days and after exposure to trace water by the addition of a single drop of ethanol containing <0.2% (wt %) of water to a toluene dispersion. The 5 days of air exposure decreased the quantum yield by more than 50% and shifted the peak emission to a slightly shorter wavelength, both indicative of surface oxidation.[55] The addition of trace water to the nanocrystals had an even more dramatic effect on the nanocrystals because it immediately quenched the PL of the sample. The Supporting Information contains a video of this observation along with a comparison to alkene-passivated Si nanocrystals. The Si−S bonded capping ligands are highly susceptible to hydrolysis. Thiol capping of Si is quite different than germanium (Ge), whereas dodecanethiol-passivated Ge nanowires are very stable, even when submerged in boiling water.[56]

Dodecanethiol-capping ligands could also be exchanged with alkenes by heating in 1-dodecene at 190 °C under nitrogen. The ligand-exchanged nanocrystals remain luminescent when exposed to water and do not undergo hydrolysis (see the video in the Supporting Information). The S 2p XPS signal is also lost after alkene repassivation (see panels a and b of Figure 9). The reverse capping ligand exchange reaction of replacing alkenes

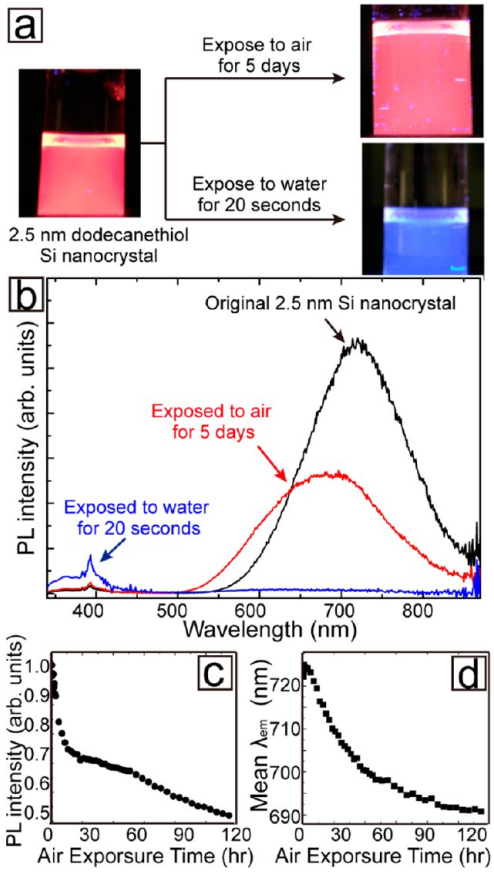

Figure 8. (a) Photographs of 2.5 nm dodecanethiol-capped Si nanocrystals dispersed in anhydrous toluene under 365 nm ultraviolet (UV) light before and after exposure to air for 5 days and after exposure to trace amount of water for 20 s (see the video in the Supporting Information also showing PL quenching upon exposure to moisture). Note that the blue color in the photograph of the sample exposed to water is just the reflection from the UV lamp and not PL from the nanocrystals. (b) PL emission spectra (λ_{exc} = 320 nm) of 2.5 nm dodecanethiol-capped Si nanocrystals dispersed in anhydrous toluene before (black curve) and after exposure to air for 5 days (red curve) and water for 20 s (blue curve). (c) Integrated PL intensity measured for 2.5 nm dodecanethiol-capped Si nanocrystals exposed to air. The PL quantum yield drops by 50% in 5 days. (d) Plot of the average PL emission wavelength of 2.5 nm dodecanethiol-capped Si nanocrystal against the time that the sample was exposed to air, showing a 35 nm blue shift in 5 days.

with thiols does not occur. For instance, heating dodecene-capped Si nanocrystal in 1-dodecanethiol does not lead to a reappearance of the S 2p XPS signal (see panels c and d of Figure 9). The mechanism of this replacement reaction requires further study. A source of hydrogen is required, and although the Si−C bond energy (318 kJ/mol) is higher than the Si−S bond energy (293 kJ/mol), the difference is not particularly significant and the reverse exchange might also be expected. Most likely, the kinetic barrier to Si−S bond cleavage, especially in the presence of any trace moisture, is significantly lower than it is for Si−C bond cleavage.

Mechanism of Thermally Induced Thiolation of Si Nanocrystals. Two alternative mechanisms, illustrated in Figure 10, are proposed to explain the passivation of Si nanocrystal surfaces by thermally promoted thiolation. One pathway is similar to the thermally initiated radical reaction for hydrosilylation, in which the Si−H bond on the Si nanocrystal

DOI: 10.1021/acs.langmuir.5b01246
Langmuir 2015, 31, 6886−6893

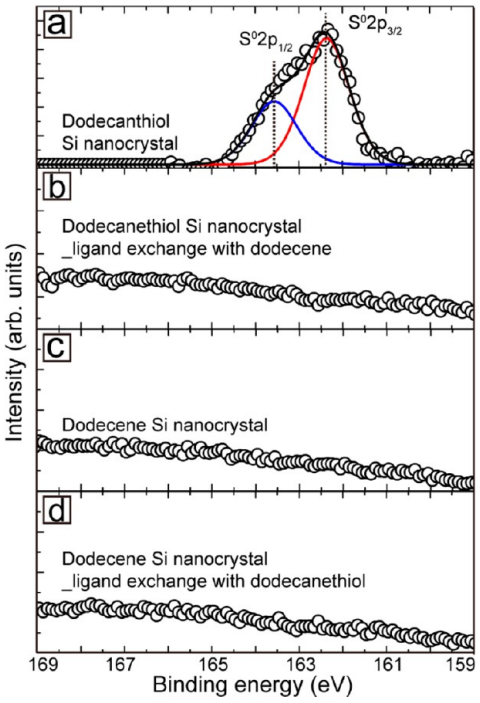

Figure 9. XPS S 2p signal of (a) dodecanethiol-capped Si nanocrystal and (b) same sample heated in 1-dodecene, showing successful ligand exchange from dodecanethiol to dodecene. XPS S 2p signal of (c) dodecene-capped Si nanocrystal and (d) same sample heated in 1-dodecanethiol, showing no evidence of ligand exchange from dodecene to dodecanethiol.

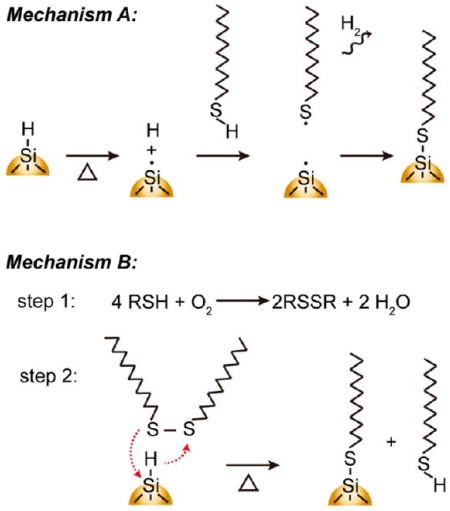

Figure 10. Proposed mechanisms for thermally-induced thiolation of hydride-terminated Si nanocrystals.

surface is cleaved at elevated temperature to yield silyl radicals and hydrogen radicals that react with thiol to evolve H_2 gas and thiol radicals,[57,58] which finally react with silyl radicals to generate Si−S bonds. An alternative mechanism involves the oxidation of thiols (RSH) by residual O_2 to create disulfides (RS−SR), which are reduced and cleaved by silicon hydride (Si−H) on the surface of Si nanocrystal through the reaction RS−SR + Si−H → RS−Si + RSH, similar to the reaction between disulfide and sodium borohydride[55] and sodium hydride.[59,60]

CONCLUSION

Dodecanethiol provides effective capping ligand passivation of Si nanocrystals, provided that water exposure is avoided. The Si−S bond is relatively stable to oxidation in the presence of dry air, and under inert conditions, the thiol-capped nanocrystals exhibit PL similar to alkene-passivated Si nanocrystals. FTIR spectroscopy and XPS confirmed that the alkanethiol ligands are covalently bonded to the Si nanocrystals. Although thiols do not provide the stability against oxidation that alkenes can provide, they offer a route to ligand exchange for Si nanocrystals.

ASSOCIATED CONTENT

Supporting Information

Movie of fluorescing Si nanocrystals passivated with dodecene or dodecanethiol in the presence of moisture (AVI), Debye−Scherrer analysis of nanocrystal size, S 2p XPS data for dodecanethiol-capped Si nanocrystals exposed to air, TEM images of hydride-terminated Si nanocrystals, and PL stability of dodecanethiol-capped Si nanocrystals in air (PDF). The Supporting Information is available free of charge on the ACS Publications website at DOI: 10.1021/acs.langmuir.5b01246.

AUTHOR INFORMATION

Corresponding Author

*Telephone: +1-512-471-5633. Fax: +1-512-471-7060. E-mail: korgel@che.utexas.edu.

Notes

The authors declare no competing financial interest.

ACKNOWLEDGMENTS

Financial support of this work was received from the Robert A. Welch Foundation (Grant F-1464) and the National Science Foundation (Grant CHE-1308813). This work was performed, in part, at the Center for Nanoscale Materials, an Office of Science user facility, which was supported by the Office of Basic Energy Sciences, Office of Science, U.S. Department of Energy, under Contract DE-AC02-06CH11357. The authors thank Hugo Celio of the Texas Materials Institute at The University of Texas at Austin for building the air-free interface/capsule for material transfer to the XPS.

REFERENCES

(1) Streetman, B.; Banerjee, S. *Solid State Electronic Devices*, 7th ed.; Prentice Hall: Upper Saddle River, NJ, 2015.

(2) Mastronardi, M. L.; Henderson, E. J.; Puzzo, D. P.; Ozin, G. A. Small silicon, big opportunities: The development and future of colloidally-stable monodisperse silicon nanocrystals. *Adv. Mater.* **2012**, *24*, 5890−5898.

(3) Hessel, C. M.; Reid, D.; Panthani, M. G.; Rasch, M. R.; Goodfellow, B. W.; Wei, J.; Fujii, H.; Akhavan, V.; Korgel, B. A. Synthesis of ligand-stabilized silicon nanocrystals with size-dependent photoluminescence spanning visible to near-infrared wavelengths. *Chem. Mater.* **2012**, *24*, 393−401.

(4) Brus, L. Luminescence of silicon materials: Chains, sheets, nanocrystals, nanowires, microcrystals, and porous silicon. *J. Phys. Chem.* **1994**, *98*, 3575−3581.

(5) Wilson, W. L.; Szajowski, P. F.; Brus, L. E. Quantum confinement in size-selected, surface-oxidized silicon nanocrystals. *Science* **1993**, *262*, 1242−1244.

(6) Erogbogbo, F.; Yong, K.-T.; Roy, I.; Xu, G.; Prasad, P. N.; Swihart, M. T. Biocompatible luminescent silicon quantum dots for imaging of cancer cells. *ACS Nano* **2008**, *2*, 873−878.

DOI: 10.1021/acs.langmuir.5b01246
Langmuir 2015, 31, 6886−6893

(7) Park, J.-H.; Gu, L.; Von Maltzahn, G.; Ruoslahti, E.; Bhatia, S. N.; Sailor, M. J. Biodegradable luminescent porous silicon nanoparticles for *in vivo* applications. *Nat. Mater.* **2009**, *8*, 331−336.
(8) Singh, V.; Yu, Y.; Sun, Q.-C.; Korgel, B. A.; Nagpal, P. Pseudo-direct bandgap transitions in silicon nanocrystals: Effect on optoelectronics and thermoelectrics. *Nanoscale* **2014**, *6*, 14643−14647.
(9) Erogbogbo, F.; Yong, K.-T.; Hu, R.; Law, W.-C.; Ding, H.; Chang, C.-W.; Prasad, P. N.; Swihart, M. T. Biocompatible magnetofluorescent probes: Luminescent silicon quantum dots coupled with superparamagnetic iron(III) oxide. *ACS Nano* **2010**, *4*, 5131−5138.
(10) Hessel, C. M.; Rasch, M. R.; Hueso, J. L.; Goodfellow, B. W.; Akhavan, V. A.; Puvanakrishnan, P.; Tunnel, J. W.; Korgel, B. A. Alkyl passivation and amphiphilic polymer coating of silicon nanocrystals for diagnostic imaging. *Small* **2010**, *6*, 2026−2034.
(11) Cheng, K.-Y.; Anthony, R.; Kortshagen, U. R.; Holmes, R. J. Hybrid silicon nanocrystal−organic light-emitting devices for infrared electroluminescence. *Nano Lett.* **2010**, *10*, 1154−1157.
(12) Puzzo, D. P.; Henderson, E. J.; Helander, M. G.; Wang, Z.; Ozin, G. A.; Lu, Z. Visible colloidal nanocrystal silicon light-emitting diode. *Nano Lett.* **2011**, *11*, 1585−1590.
(13) Jiang, C.-W.; Green, M. A. Silicon quantum dot superlattices: Modeling of energy bands, densities of states, and mobilities for silicon tandem solar cell applications. *J. Appl. Phys.* **2006**, *99*, 114902.
(14) Priolo, F.; Gregorkiewicz, T.; Galli, M.; Krauss, T. F. Silicon nanostructure for photonics and photovoltaics. *Nat. Nanotechnol.* **2014**, *9*, 19−32.
(15) Beard, M. C.; Knutsen, K. P.; Yu, P.; Luther, J. M.; Song, Q.; Metzger, W. K.; Ellingson, R. J.; Nozik, A. J. Multiple exciton general in colloidal silicon nanocrystals. *Nano Lett.* **2007**, *7*, 2506−2512.
(16) Guo, L.; Leobandung, E.; Chou, S. Y. A silicon single-electron transistor memory operating at room temperature. *Science* **1997**, *275*, 649−651.
(17) Pereira, R. N.; Niesar, S.; You, W. B.; da Cunha, A. F.; Erhard, N.; Stegner, A. R.; Wiggers, H.; Willinger, M.-G.; Stutzmann, M.; Brandt, M. S. Solution-processed networks of silicon nanocrystals: The role of internanocrystal medium on semiconducting behavior. *J. Phys. Chem. C* **2011**, *115*, 20120−20127.
(18) Tu, C.-C.; Zhang, Q.; Lin, L. Y.; Cao, G. Brightly photoluminescence phosphor materials based on silicon quantum dots with oxide shell passivation. *Opt. Express* **2012**, *20*, A69−A74.
(19) *Silicon Nanocrystals: Fundamentals, Synthesis and Applications*; Pavesi, L., Turan, R., Eds.; Wiley-VCH: Weinheim, Germany, 2010.
(20) Steigerwald, M. L.; Alivisatos, A. P.; Gibson, J. M.; Harris, T. D.; Kortan, R.; Muller, A. J.; Thayer, A. M.; Duncan, T. M.; Douglass, D. C.; Brus, L. E. Surface derivatization and isolation of semiconductor cluster molecules. *J. Am. Chem. Soc.* **1988**, *110*, 3046−3050.
(21) Alivisatos, A. P. Semiconductor clusters, nanocrystals, and quantum dots. *Science* **1996**, *271*, 933−937.
(22) Yu, Y.; Hessel, C. M.; Bogart, T. D.; Panthani, M. G.; Rasch, M. R.; Korgel, B. A. Room temperature hydrosilylation of silicon nanocrystals with bifunctional terminal alkenes. *Langmuir* **2013**, *29*, 1533−1540.
(23) Yang, Z.; Iabal, M.; Dobbie, A. R.; Veinot, J. G. C. Surface-induced alkene oligomerization: Does thermal hydrosilylation really lead to monolayer protected silicon nanocrystals? *J. Am. Chem. Soc.* **2013**, *135*, 17595−17601.
(24) Kelly, J. A.; Henderson, E. J.; Clark, R. J.; Hessel, C. M.; Cavell, R. G.; Veinot, J. G. C. X-ray absorption spectroscopy of functionalized silicon nanocrystals. *J. Phys. Chem. C* **2010**, *114*, 22519−22525.
(25) Miller, J. B.; Van Sickle, A. R.; Anthony, R. J.; Kroll, D. M.; Kortshagen, U. R.; Hobbie, E. K. Ensemble brightening and enhanced quantum yield in size-purified silicon nanocrystals. *ACS Nano* **2012**, *6*, 7389−7396.
(26) Mastronardi, M. L.; Maier-Flaig, F.; Faulkner, D.; Henderson, E. J.; Kübel, C.; Lemmer, U.; Ozin, G. A. Size-dependent absolute quantum yields for size-separated colloidally-stable silicon nanocrystals. *Nano Lett.* **2012**, *12*, 337−342.
(27) Li, X.; He, Y.; Swihart, M. T. Surface functionalization of silicon nanoparticles produced by laser-driven pyrolysis of silane followed by HF−HNO_3 etching. *Langmuir* **2004**, *20*, 4720−4727.
(28) Lu, X.; Hessel, C. M.; Yu, Y.; Bogart, T. D.; Korgel, B. A. Colloidal luminescent silicon nanorods. *Nano Lett.* **2013**, *13*, 3101−3105.
(29) Yu, Y.; Bosoy, C. A.; Hessel, C. M.; Smilgies, D.-M.; Korgel, B. A. Silicon nanocrystal superlattices. *ChemPhysChem* **2013**, *14*, 84−87.
(30) Locritani, M.; Yu, Y.; Bergamini, G.; Baroncini, M.; Molloy, J. K.; Korgel, B. A.; Ceroni, P. Silicon nanocrystals functionalized with pyrene units: Efficient-harvesting antennae with bright near-infrared emission. *J. Phys. Chem. Lett.* **2014**, *5*, 3325−3329.
(31) Heitsch, A. T.; Hessel, C. M.; Akhavan, V. A.; Korgel, B. A. Colloidal silicon nanorod synthesis. *Nano Lett.* **2009**, *9*, 3042−3047.
(32) Heitsch, A. T.; Akhavan, V. A.; Korgel, B. A. Rapid SFLS synthesis of Si nanowires using trisilane with in situ alkyl-amine passivation. *Chem. Mater.* **2011**, *23*, 2697−2699.
(33) Lu, X.; Korgel, B. A. A single-step reaction for silicon and germanium nanorods. *Chem.—Eur. J.* **2014**, *20*, 5874−5879.
(34) Dasog, M.; Veinot, J. G. C. Size independent blue luminescence in nitrogen passivated silicon nanocrystals. *Phys. Status Solidi A* **2012**, *209*, 1844−1846.
(35) Dasog, M.; De los Reyes, G. B.; Titova, L. V.; Hegmann, F. A.; Veinot, J. G. C. Size vs surface: Tuning the photoluminescence of freestanding silicon nanocrystals across the visible spectrum via surface groups. *ACS Nano* **2014**, *8*, 9636−9648.
(36) Dasog, M.; Yang, Z.; Regli, S.; Atkins, T. M.; Faramus, A.; Singh, M. P.; Muthuswamy, E.; Kauzlarich, S. M.; Tilley, R. D.; Veinot, J. G. C. Chemical insight into the origin of red and blue photoluminescence arising from freestanding silicon nanocrystals. *ACS Nano* **2013**, *7*, 2676−2685.
(37) Lee, D. C.; Smith, D. K.; Heitsch, A. T.; Korgel, B. A. Colloidal magnetic nanocrystals: Synthesis, properties and applications. *Annu. Rep. Prog. Chem., Sect. C: Phys. Chem.* **2007**, *103*, 351−402.
(38) Sardar, R.; Funston, A. M.; Mulvaney, P.; Murray, R. W. Gold nanoparticles: Past, present, and future. *Langmuir* **2009**, *25*, 13840−13851.
(39) Desireddy, A.; Conn, B. E.; Guo, J.; Yoon, B.; Barnett, R. N.; Monahan, B. M.; Kirschbaum, K.; Griffith, W. P.; Whetten, R. L.; Landman, U.; Bigioni, T. P. Ultrastable silver nanoparticles. *Nature* **2013**, *501*, 399−402.
(40) Nosaka, Y.; Yamaguchi, K.; Miyama, H.; Hayashi, H. Preparation of size-controlled CdS colloids in water and their optical properties. *Chem. Lett.* **1988**, *17*, 605−608.
(41) Liang, L.; Pandey, A.; Werder, D. J.; Khanal, B. P.; Pietryga, J. M.; Klimov, V. I. Efficient synthesis of highly luminescent copper indium sulfide-based core/shell nanocrystals with surprisingly long-lived emission. *J. Am. Chem. Soc.* **2011**, *133*, 1176−1179.
(42) Hessel, C. M.; Henderson, E. J.; Veinot, J. G.C. Hydrogen silsesquioxane: A molecular precursor for nanocrystalline Si−SiO_2 composites and freestanding hydride-surface-terminated silicon nanoparticles. *Chem. Mater.* **2006**, *18*, 6139−6146.
(43) Panthani, M. G.; Hessel, C. M.; Reid, D.; Casillas, G.; José-Yacamán, M.; Korgel, B. A. Graphene-supported high-resolution TEM and STEM imaging of silicon nanocrystals and their capping ligands. *J. Phys. Chem. Lett.* **2012**, *116*, 22463−22468.
(44) Kelly, J. A.; Shukaliak, A. M.; Fleischauer, M. D.; Veinot, J. G. C. Size-dependent reactivity in hydrosilylation of silicon nanocrystals. *J. Am. Chem. Soc.* **2011**, *133*, 9564−9571.
(45) Socrates, G. *Infrared Characteristic Group Frequencies*, 2nd ed.; John Wiley & Sons: London, U.K., 1994.
(46) Lucovsky, G.; Nemanich, R. J.; Knights, J. C. Structural interpretation of the vibrational spectra of α-Si:H alloys. *Phys. Rev. B: Condens. Matter Mater. Phys.* **1979**, *19*, 2064−2073.
(47) Although the vibration observed for 1-dodecanethiol between 2600 and 2550 cm^{-1} is relatively weak, it is recognized fairly easily when present because this spectral region is relatively free of other absorption bands.[45]

DOI: 10.1021/acs.langmuir.5b01246
Langmuir 2015, 31, 6886−6893

(48) Joseph, Y.; Besnard, I.; Rosenberger, M.; Guse, B.; Nothofer, H.-G.; Wessels, J. M.; Wild, U.; Knop-Gericke, A.; Su, D.; Schlögl, R.; Yasuda, A.; Vossmeyer, T. Self-assembled gold nanoparticle/alkanethiol films: Preparation, electron microscopy, XPS-analysis, charge transport, and vapor-sensing properties. *J. Phys. Chem. B* **2003**, *107*, 7406−7413.
(49) Castner, D. G. X-ray photoelectron spectroscopy sulfur 2p study of organic thiol and disulfide binding interactions with gold surfaces. *Langmuir* **1996**, *12*, 5083−5086.
(50) Bourg, M.-C.; Badia, A.; Lennox, R. B. Gold−sulfur bonding in 2D and 3D self-assembled monolayers: XPS characterization. *J. Phys. Chem. B* **2000**, *104*, 6552−6567.
(51) Hostetler, M. J.; Wingate, J. E.; Zhong, C.-J.; Harris, J. E.; Vachet, R. W.; Clark, M. R.; Londono, J. D.; Green, S. J.; Stokes, J. J.; Wignall, G. D.; Glish, G. L.; Porter, M. D.; Evans, N. D.; Murray, R. W. Alkanethiolate gold cluster molecules with core diameters from 1.5 to 5.2 nm: Core and monolayer properties as a function of core size. *Langmuir* **1998**, *14*, 17−30.
(52) Lai, Y.-H.; Yeh, C.-T.; Lin, Y.-H.; Hung, W.-H. Adsorption and thermal decomposition of H_2S on Si(100). *Surf. Sci.* **2002**, *519*, 150−156.
(53) Haas, A. The chemistry of silicon−sulfur compounds. *Angew. Chem., Int. Ed.* **1965**, *4*, 1014−1023.
(54) Sommer, L. H.; McLick, J. Stereochemistry of asymmetric silicon. IX. The silicon−sulfur bond. *J. Am. Chem. Soc.* **1967**, *89*, 5806−5812.
(55) Crestfield, A. M.; Moore, S.; Stein, W. H. The preparation and enzymatic hydrolysis of reduced and S-carboxymethylated proteins. *J. Biol. Chem.* **1963**, *238*, 622−627.
(56) Holmberg, V. C.; Korgel, B. A. Corrosion resistance of thiol- and alkene-passivated germanium nanowires. *Chem. Mater.* **2010**, *22*, 3698−3703.
(57) Armstrong, D. A.; Wilkening, V. G. Effects of pH in the γ-radiolysis of aqueous solutions of cysteine and methyl mercaptan. *Can. J. Chem.* **1964**, *42*, 2631−2635.
(58) Patai, S. *The Chemistry of the Thiol Group*; John Wiley & Sons: London, U.K., 1974.
(59) Krull, L. H.; Friedman, M. Reduction of protein disulfide bonds by sodium hydride in dimethyl sulfoxide. *Biochem. Biophys. Res. Commun.* **1967**, *29*, 373−377.
(60) Wall, J. S. Disulfide bonds: Determination, location, and influences on molecular properties of proteins. *J. Agric. Food Chem.* **1971**, *19*, 619−625.

DOI: 10.1021/acs.langmuir.5b01246
Langmuir 2015, 31, 6886−6893